Role of manifolds in the transport of chaotic trajectories in the standard nontwist map

Michele Mugnaine [*]
Lorena School of Engineering (EEL-USP), University of São Paulo, Lorena, SP 12.602-810, Brazil

Matheus Rolim Sales and Edson Denis Leonel
São Paulo State University (UNESP), Institute of Geosciences and Exact Sciences, Rio Claro, SP 13506-900, Brazil

Iberê Luiz Caldas
Institute of Physics, University of São Paulo, São Paulo, SP 05508-900, Brazil

José Danilo Szezech Jr.
Department of Mathematics and Statistics, State University of Ponta Grossa, Ponta Grossa, PR 84030-900, Brazil

(Received 9 April 2026; accepted 26 June 2026; published 24 July 2026)

A crucial question in transport theory is determining the critical parameter values at which abrupt changes in phase space occur. In nontwist Hamiltonian systems, this transition is associated with the breakup of the shearless curve. Ideally, once this curve is destroyed, chaotic trajectories should cross the barrier freely. A direct way to characterize this process is to compute the number of crossing trajectories to determine the transmission through the phase space. However, in this work, we show that nonzero transmission is not an immediate consequence of the disappearance of the shearless curve. By computing the parameter space for the existence of the shearless curve and evaluating the transmissivity, we identify regions where transport is zero even in the absence of a complete barrier. Consequently, relying solely on zero transmission leads to inaccurate values for the barrier breakup. By analyzing the underlying invariant manifolds, we show how turnstiles and torus free barriers strongly influence the gap between the breakup of the shearless curve and the onset of positive transport. Furthermore, we investigate how these regions depend on the island periodicity and analyze their evolution as a function of the iteration time. Our results reveal distinct power-law exponents for the decay of the size of the region with no barrier and no transport in the parameter space. The different behaviors for odd and even periods reflect differences in the efficiency of turnstile mechanisms and torus free barriers.

DOI: 10.1103/28br-cb3m

I. INTRODUCTION

In nonintegrable Hamiltonian systems, the coexistence of regular and chaotic dynamics is a typical feature. Consequently, the dynamics is neither entirely regular nor entirely chaotic; rather, it depends sensitively on the initial condition [1]. The motion of chaotic trajectories in phase space, also known as transport, can be reduced or even prevented by total and partial transport barriers—such as invariant curves, cantori, and manifold structures—as turnstiles and torus free barriers [2–8]. A major question in transport studies is when the last torus breaks, and more specifically, for which critical parameter values this occurs. The knowledge of these critical values should, *a priori*, determine the connection of chaotic regions and the transport along the phase space.

According to the Kolmogorov-Arnold-Moser (KAM) theorem, when an integrable system is perturbed, a finite fraction of invariant tori persists, while others are destroyed and replaced by chaotic behavior [1]. The prevalence of invariant curves is related to its irrationality, in the sense that curves that survive stronger perturbations are more irrational, i.e., their rotation numbers are harder to approximate by rational numbers [1]. For the Chirikov standard map [9], the breakup of the invariant torus (or KAM curves) with a rotation number equal to the golden ratio is one of the most classic problems in nonlinear dynamics and KAM theory. The golden ratio, $\omega = (\sqrt{5}-1)/2$, characterizes the most "robust" or irrational curve of the system. It is the last global invariant curve to be destroyed as the nonlinearity parameter increases. The determination of this critical value is determined by techniques like the residue and the mean residue to determine the stability of the orbits [10], by using renormalization group theory and through the connection between invariant circles and the renormalization operator [11]. However, even after the breakup, the golden ratio torus does not completely disappear but transforms into an invariant Cantor set (cantori), which acts as a partial barrier to chaotic transport [2,12]. The reader can refer to Ref. [13] and references therein, where a detailed and historical review of these concepts applied in twist maps is presented.

Twist maps satisfy the twist condition globally, and the KAM theorem can therefore be used to study transport barriers in these systems. However, the same is not true for

[*]Contact author: mugnaine@usp.br

nontwist maps. For a two-dimensional map $(x_{n+1}, y_{n+1}) = M(x_n, y_n)$, the twist condition is defined by $\frac{\partial x_{n+1}}{\partial y_n} \neq 0$ and it must be satisfied at all points in phase space for the system to be considered a twist map. For nontwist systems, the twist condition is not satisfied throughout the entire phase space and, in a system expressed in action-angle variables, the rotation number profile exhibits a nonmonotonic dependence on the action, exhibiting local extrema at specific points. A paradigmatic nontwist map is the standard nontwist map (SNM), introduced by del-Castillo-Negrete and Morrison [14]. The SNM is a simple nontwist system that exhibits particular features, such as a nonmonotonic rotation number profile, the formation of twin island chains, and reconnection and collision scenarios of regular orbits [6,14–16]. Among the invariant solutions of the SNM, the shearless curve is of particular interest, as it corresponds to the extremum of the rotation number profile. The shearless curve is a robust structure; i.e., it survives under strong perturbations. Unlike twist systems, there is no rigorous proof regarding the last remaining invariant curve; however, in most studies, it is assumed to be the shearless curve [17].

The SNM is a reversible map (it can be factored into a product of involutions) and it possesses specific spatial and time-reversal symmetries. These symmetries give rise to special points, known as indicator points, which are mathematically guaranteed to lie on the shearless invariant curve [17–19]. This property enables the determination of the breakup of the shearless curve [17,20,21], providing an alternative for the KAM theorem in nontwist maps.

From a transport perspective, it is also possible to identify the parameter values for which a barrier exists by computing the transmissivity. Transmissivity is defined as the fraction of orbits that cross phase space within a given time [4]. If the transmissivity is null, a barrier can be identified in phase space. As reported in our previous works [6,7], the presence of partial barriers, as Cantori, turnstiles, and torus free barriers, can suppress transport or require long iteration times for a nonzero transmissivity to be observed. Torus free barriers, in particular, can act as strong partial barriers. In Ref. [7], we showed that the dipole configuration of the manifolds significantly reduces the passage of chaotic trajectories, leading to a scenario of zero transport even for long iteration times. This leads to the occurrence of "false positives," where cases with very strong partial barriers are interpreted as phase spaces with a complete transport barrier.

Although we identified the manifold structures and how chaotic trajectories cross them in Refs. [6,7], it is still not completely clear what the impact is of these false positives in the study of transport barriers in nontwist maps, nor the causes of this scenario. In this work, we analyze the parameter space of the SNM for the existence of the shearless curve together with the study of transmissivity. By identifying the false positives, i.e., the no-barrier, no-transport regions, we investigate what leads to this behavior. We also analyze the manifold structures and identify the relation between these structures and the absence of transmissivity. Finally, we study the prevalence of the no-barrier, no-transport regions for different iteration times, which provides insight into the robustness of partial barriers.

Our paper is organized as follows. In Sec. II we present the standard nontwist map and the evaluation of the parameter space for the existence of the shearless curve, as well as the transmissivity for different final iteration times. The analysis of the no-barrier, no-transport regions is discussed in Sec. III. The manifold structures of partial barrier are described in Sec. IV, while their robustness is analyzed in Sec. V. Our concluding remarks are presented in Sec. VI.

II. TRANSPORT BARRIERS AND TRANSMISSIVITY

Two-dimensional conservative systems can be modeled by area preserving maps with the general form

$$\begin{aligned} x_{n+1} &= x_n + \Omega(y_{n+1}) + f(x_n, y_{n+1}), \\ y_{n+1} &= y_n + g(x_n, y_{n+1}). \end{aligned} \tag{1}$$

These maps are often applied in the analysis of nonintegrable Hamiltonian systems, composed by an integrable system under the effect of a nonintegrable perturbation [1,15]. In order to represent a conservative systems, the condition $\frac{\partial f}{\partial x_n} + \frac{\partial g}{\partial y_{n+1}} = 0$ must be satisfied. The function Ω represents the frequency of the unperturbed Hamiltonian while the functions f and g are identified as the perturbation terms [15].

Among area preserving maps, there exists a class of maps, called *nontwist maps*, for which the twist condition, defined by [1]

$$\frac{\partial x_{n+1}}{\partial y_n} \neq 0, \tag{2}$$

is not satisfied at all points (x, y) in the phase space. The violation of the twist condition leads to particular types of bifurcations, such as orbit collisions and separatrix reconnections, as well as to the existence of twin chains of islands and a shearless curve, which is a robust invariant curve in the phase space [15].

A simple map that reproduces the properties of nontwist systems is the *standard nontwist map* (SNM), proposed by del-Castillo-Negrete and Morrison [14] and defined as

$$\begin{aligned} y_{n+1} &= y_n - b\sin(2\pi x_n), \\ x_{n+1} &= x_n + a\left(1 - y_{n+1}^2\right), \ \bmod 1, \end{aligned} \tag{3}$$

where x and y are canonically conjugate variables, with $y \in \mathbb{R}$ and $x \in [0, 1)$. The parameters a and b are real, independent, and are related with the nonmonotonic aspect of the system and the perturbation amplitude, respectively. Since Eq. (3) is a nontwist map, its rotation number profile is nonmonotonic with respect to the variable y. Bifurcations, the route to chaos and transport properties in this map, were extensively studied in, e.g., Refs. [4–7,15,20,22–24]. As a nonintegrable Hamiltonian system, the SNM exhibits coexistence of chaos and regularity in phase space, and its transport properties are not easily predictable. As discussed in Refs. [4–7,20] the movement of chaotic trajectories in the phase space is affected by total barriers, as the shearless curve, or by partial barriers, formed by manifold structures such as turnstiles or torus free barriers. In Fig. 1, we present three different scenarios of transport barriers in the SNM: (a) total barrier, (b) strong partial barrier, (c) weak partial barrier. Additionally, we present

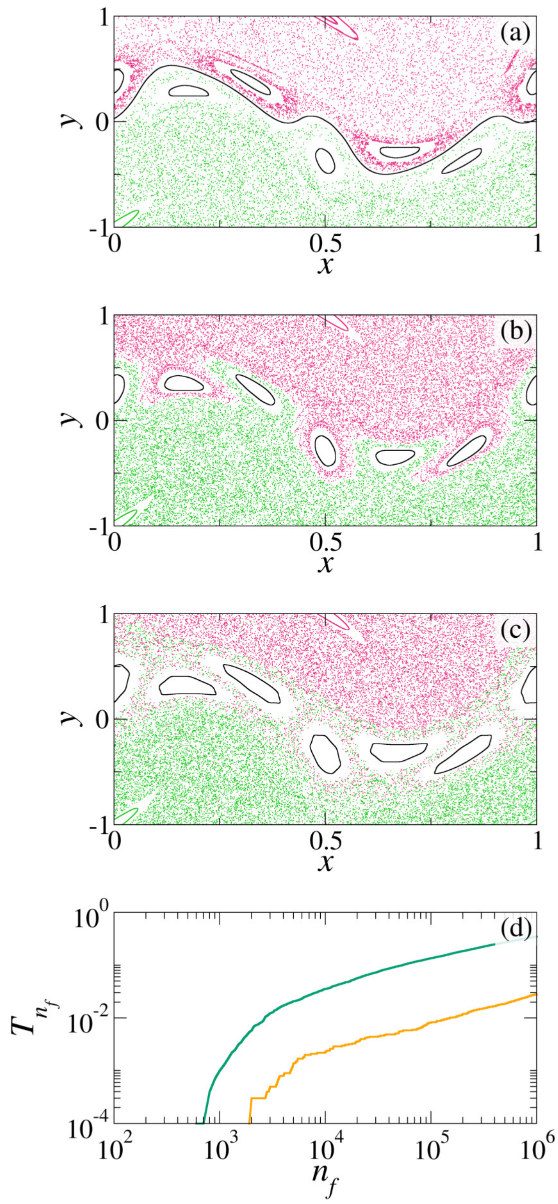

FIG. 1. Phase spaces corresponding to three scenarios of transport barriers. In (a), the parameters are $a = 0.38$ and $b = 0.75$ and we observe a total transport barrier, represented by the central black curve. For panel (b), we have $a = 0.37$ and $b = 0.75$ and a strong partial barrier, as the pink and green solutions do not mix. In (c), for $a = 0.375$ and $b = 0.75$, the partial barrier is weaker, allowing mixing between the chaotic trajectories. The transmissivity T_{n_f} for the scenarios (b),(c), as a function of the final iteration time, is shown in panel (d). The curves corresponding to scenarios (b),(c) are shown in orange and teal, respectively.

the value of the transmissivity T_{n_f} for cases (b) and (c) for different final iteration times.

To construct the phase spaces of Fig. 1, we choose 50 initial condition in $y = \pm 1$ and iterate all of them for 10^4 iterations. The solutions from the initial conditions in $y = 1$ ($y = -1$) are marked in pink (green). The black curves represent invariant solutions as the regular islands in the three panels of Fig. 1 and the shearless curve in Fig. 1(a).

TABLE I. Transmissivity values T_{n_f} for the parameters of Fig. 1 and different iteration times n_f.

Fig. 1 \ n_f	10^2	10^3	10^4	10^5	10^6
(a)	0	0	0	0	0
(b)	0	0	0.0023	0.0082	0.0279
(c)	0	0.0010	0.0355	0.1357	0.3491

As we can observe in Fig. 1(a), there is no mixing between the green and pink points. This is explained by the existence of a total barrier, indicated by the black central curve. In Fig. 1(b), we no longer observe a total barrier; however, the pink and green chaotic trajectories do not mix for 10^4 iterations, indicating the presence of an effective partial barrier. It was shown in Refs. [4–6] that the partial barrier is formed by a specific manifold structure, known as intracrossing, in which the turnstiles associated with different chains of hyperbolic points do not intersect. A different scenario is observed in Fig. 1(c), where mixing between the chaotic trajectories occurs, especially around the regular islands. In this case, an effective partial barrier is no longer present, and transport in phase space is enhanced.

A way to quantify the transport through the partial barriers in the phase space is via the transmissivity, defined as the fraction of orbits that cross the barrier in a given time [4]. In order to compute the transmissivity, we distribute 10^4 initial conditions along the line $y = -10$, iterate them for different numbers of iteration, and compute how many trajectories cross the phase space and reach the line $y = 10$. The ratio between the number of trajectories that cross the phase space and the total number of initial conditions is the transmissivity T_{n_f} for a final iteration time n_f. For the SNM, the islands are typically located around $y = 0$. However, for smaller values of a, the islands tend to become larger, and regular solutions can be found for greater values of $|y|$. For this reason, we chose the line $y = -10$ for the initial conditions in order to avoid the influence of regular solutions in the computation of the transmissivity.

Following this method, we compute the transmissivity for the three parameter sets of Fig. 1 and different iteration times. The results are presented in Table I.

As expected, for the parameters of the phase space of Fig. 1(a), the transmissivity is null for all the iteration times. Due to the uniqueness of solutions, chaotic trajectories cannot cross regular structures, such as invariant curves, and therefore transport is zero, independently of the iteration time. For the parameters of Fig. 1(b), the corresponding transmissivities are presented in the second row of Table I. As shown, the transport is zero for shorter iteration times, $n_f = 10^2$ and $n_f = 10^3$. For $n_f = 10^4$ we obtain a small but nonzero transmissivity and this value increases as we consider longer iteration times. A similar result is observed for the last case, corresponding to the parameters of Fig. 1(c); however, in this case, the transmissivity is already nonzero for $n_f = 10^3$. Moreover, if we compare the transmissivity values of scenarios (b) and (c) for the same iteration time, we observe that the transmissivity for scenario (c) is always larger, indicating a less effective partial transport barrier.

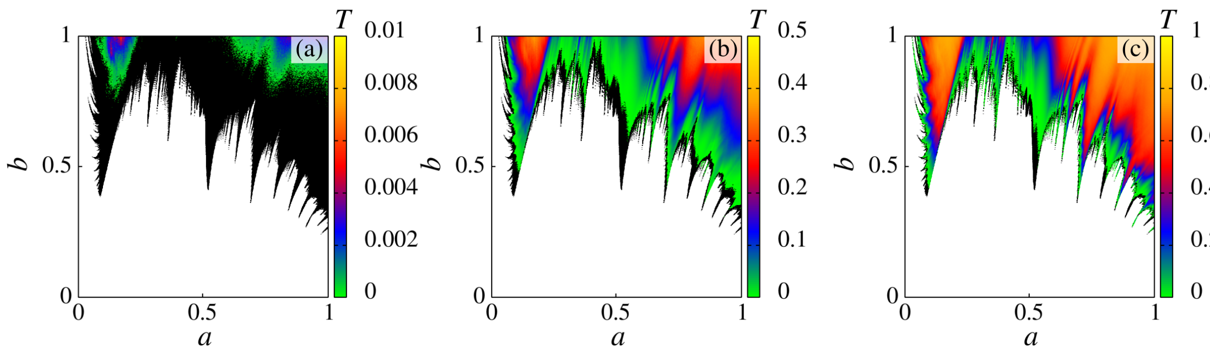

FIG. 2. Parameter space for the transmissivity T in the SNM. In all panels, the white points indicate the region where the shearless curve is present. The colored points indicate the value of the transmissivity and the black points represent a scenario where there is no shearless curve and no transport. The final iteration time is (a) $n_f = 10^2$, (b) $n_f = 10^3$, and (c) $n_f = 10^4$.

To illustrate how the transmissivity T_{n_f} increases as we consider larger n_f, we compute it over the range $n_f \in [10^2, 10^6]$. The resulting profile is shown in Fig. 1(d). We focus only on the scenarios with no barrier, i.e., scenarios (b) and (c). The curve for scenario (b) is shown in orange, while the teal curve represents scenario (c). Comparing both curves, we observe that the transmissivity increases with n_f in both cases, but the teal curve, corresponding to the scenario with a weaker partial barrier, reaches larger values, indicating a stronger transport through phase space.

From Table I and the curves in Fig. 1(d), we observe that transmissivity depends on the final iteration time and the parameters of the systems. To perform a more general analysis, we compute the transmissivity in the parameter space $a \times b$ for three different value of iteration time: $n_f = 10^2, 10^3$, and 10^4. Prior to computing the transmissivities, we identify the parameter regions where a total barrier exists and the transmissivity is always null.

To determine the parameter space for the shearless curve, we follow the method proposed by Shinohara and Aizawa in Ref. [18] based on the iteration of the indicator points. The indicator points $\mathbf{z}$ are solutions of $I_i\mathbf{z}_i = T_S\mathbf{z}_i$ where I_i are the involutions of the SNM,

$$I_0(x, y) = [-x, y - b\sin(2\pi x)],$$
$$I_1(x, y) = [-x + a(1 - y^2), y], \tag{4}$$

with $M = I_1 \circ I_0$, with M being the map (1), and T_S is the symmetry transformation [15],

$$T_S = \left(x \pm \tfrac{1}{2}, -y\right), \tag{5}$$

where $MT_S = T_SM$. Therefore, the indicator points for the SNM are

$$\mathbf{z}_0^{(0,1)} = \left(\mp\frac{1}{4}, \mp\frac{b}{2}\right), \quad \mathbf{z}_1^{(0,1)} = \left(\frac{a}{2} \mp \frac{1}{4}, 0\right). \tag{6}$$

If the indicator points belong to an invariant solution, they belong to the shearless curve [18]. If, on the other hand, they generate a chaotic trajectory, this indicates that the shearless curve no longer exists. To determine the parameter space associated with the shearless curve, we select a pair of parameters (a, b), compute the four indicator points, and iterate them for 10^6 iterations. If the resulting trajectories remain within $|y| < 10$, we conclude that the shearless curve is present in the phase space; otherwise, it has been destroyed.

By determining the region where the shearless curve exists and computing the transmissivity for all the points (a, b) in the region where the shearless curve is absent, we obtain the results presented in Fig. 2.

In all parameter spaces shown in Fig. 2, the white points represent pairs (a, b) for which the shearless curve is present and, therefore, the transmissivity is zero. In contrast, the colored points form the region where the shearless curve has been destroyed and the transmissivity is nonzero, with its magnitude indicated by the color scale. The black points correspond to parameter pairs for which the shearless curve is absent and no trajectories cross the phase space; it is a region with no barrier and no transport. They can be considered false positives, i.e., points that may be interpreted as parameters for which a total barrier exists, since no transport is observed. In this study, we focus our analysis on the black region, which indicates parameter pairs with an effective partial barrier.

By comparing the parameter spaces shown in Fig. 2, we observe that the black region decreases as we increase the final iteration time n_f. This behavior is expected, since longer iteration times increase the chances that trajectories will cross the phase space. An intriguing feature is that, in some "fingers," the black regions persist even for longer iteration times. For example, the finger near $a = 0.5$ remains black even for $n_f = 10^4$. From this, we conclude that for certain parameter pairs the partial transport barrier is more robust and persistent. In the next section, we analyze these regions in greater detail.

III. ANALYSIS OF NO-BARRIER AND NO-TRANSPORT REGIONS

As observed in the parameter spaces shown in Fig. 2, there are some regions where the black points, which indicate persistent effective partial barriers, remain prominent. In this section, we select specific regions and analyze the corresponding phase spaces, investigating the relationship between the phase space structures and the presence of effective partial barriers.

The selected regions are shown in Figs. 3(a_1)–3(a_6). The parameter space for the existence of the shearless curve is shown in light green, while the points with no barrier and no transport are displayed in black, orange, and pink for

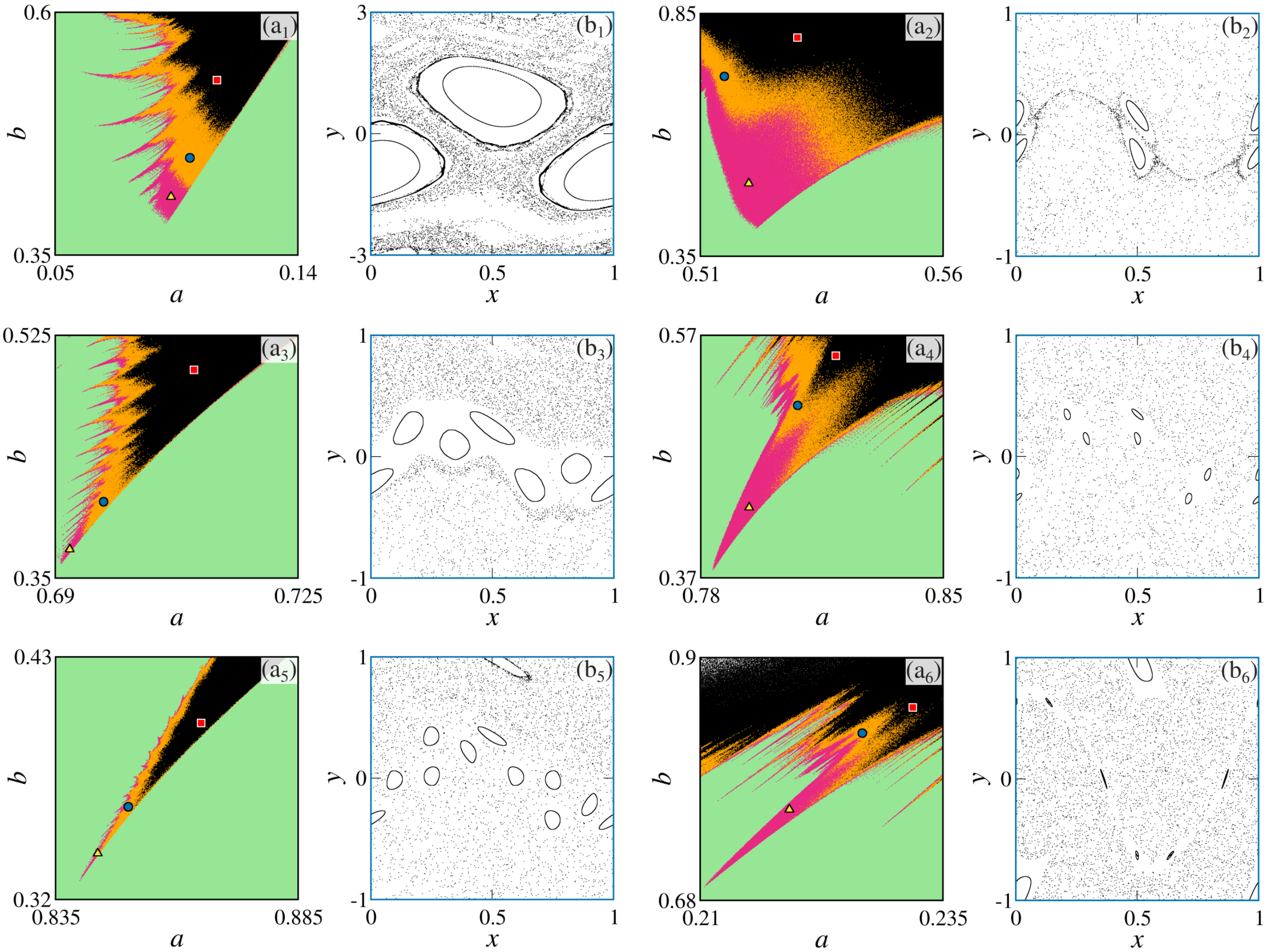

FIG. 3. Parameter space and phase space structures for different no-barrier and no-transport regions. In panels (a_1)–(a_6), we present the parameter space for the presence of shearless barrier in light green, while the no-barrier and no-transport regions are presented as black, orange, and pink points, indicating the regions for $n_f = 10^2$, 10^3, and 10^4. The blue circle in parameter space indicates the selected pair (a, b), for which the corresponding phase spaces are shown in panels (b_1)–(b_6). We observe different island periods in each selected region.

$n_f = 10^2, 10^3$, and 10^4, respectively. In the region in the parameter space where no barrier is present, we select a representative pair of parameters to plot the corresponding phase space in order to investigate its structure. The selected point is shown as a blue circle in Fig. 3(a), and the corresponding phase space is displayed in Figs. 3(b_1)–3(b_6). The scenario for the pair of parameters indicated by the red square and yellow triangle will be analyzed in the next section.

From the parameter spaces presented in Figs. 3(a_1)–3(a_6), we observe a decrease in the no-barrier, no-transport region as the final iteration time increases. The black, orange, and pink regions overlap; however, a progressive shrinkage is evident when comparing the black region with the orange one, and the orange region with the pink one. We select pairs of parameters (a, b) (the blue circles) and plot the corresponding phase space in order to investigate the island period and related structures. We observe that the islands periods range from 1 to 6 and the corresponding phase spaces are shown in Fig. 3(b_i), with $i = 1, 2, 3, 4, 5$, and 6.

By comparing all parameter spaces and associating them with the island period, we can infer that an odd period leads to a larger decrease in the no-barrier, no-transport region of parameter space. This effect is particularly evident for periods 3 and 5, as shown in Figs. 3(a_3) and 3(a_5), respectively, where the orange and pink regions are significantly smaller than the black region. In contrast, for even periods, the orange and pink regions are still smaller than the black region but they are quite similar to each other, indicating the persistence of the no-barrier, no-transport scenario for larger final iteration times n_f.

To understand the dynamical characteristics in phase space that explain this scenario, we analyze the manifolds for the cases shown in Fig. 3. The analysis is described in the next section.

IV. PARTIAL TRANSPORT BARRIERS

Considering a planar map M, we assume that M has a hyperbolic point $\mathbf{O}$ such that $\mathbf{O} = M^n(\mathbf{O})$, where n is the period of the orbit. The stable manifold W^S is defined as the set of points that approach $\mathbf{O}$ under forward iterations of the map, i.e. [25],

$$W^S = \{\mathbf{x} \in \mathbb{R}/M^k(\mathbf{x}) \to \mathbf{O} \text{ as } k \to \infty\}, \tag{7}$$

where M^k is the kth iterate of the map. Likewise, the unstable manifold W^U is defined as the set of points that approach the hyperbolic point $\mathbf{O}$ under backward iterates of the map,

$$W^U = \{\mathbf{x} \in \mathbb{R}/M^{-k}(\mathbf{x}) \to \mathbf{O} \text{ as } k \to \infty\}, \tag{8}$$

with M^{-k} being the kth iterate of the inverse map.

The unstable and stable manifolds can intersect, forming an *intracrossing* scenario in which manifolds from the same chain of hyperbolic points generate homoclinic intersections. For the nontwist map, we observe the presence of twin island chains; i.e., two islands with the same period and rotation number coexist in the phase space. Consequently, we also observe two chains of hyperbolic points. The manifolds from different hyperbolic points can also intersect, leading to an *intercrossing* scenario formed by heteroclinic intersections [4,6].

As shown in Refs. [4–7,26], the structures formed by the stable and unstable manifolds of hyperbolic points affect the transport of chaotic trajectories through phase space in nontwist maps. With this idea in mind, we perform a numerical analysis of the manifolds for parameter values selected from the parameter spaces in Fig. 3, in order to explain the differences in the size of the no-transport, no-barrier regions for different periods of the twin islands.

For this analysis, we select three points in the parameter space in the no-barrier region, one for each final iteration time, i.e., one for the black, orange, and pink regions . The selected points are indicated by the red square, blue circle, and yellow triangle in Fig. 3. We then follow the computation method presented in Ref. [25] and compute the stable and unstable manifold for each hyperbolic points chain. We perform this computation for every parameter space shown in Fig. 3. Here, we present the results for periods 2, 3, and 5. The other periods exhibit similar scenarios. The respective manifolds for such periods are shown in Figs. 4–6.

The manifold structures for the even-period cases are represented by the period-2 case, shown in Fig. 4. We choose to show a magnification around a pair of islands in order to highlight the details of the structure. In all panels of Fig. 4, we observe two hyperbolic points, $\mathbf{O}^{\blacktriangle}$ and $\mathbf{O}^{\blacksquare}$, indicated by the black triangle and black square, respectively. From each hyperbolic point, the stable and unstable manifolds emerge and they form a dipolar structure named *torus free barrier* [7]. This type of barrier is known to be a robust partial barrier, requiring long iteration times for chaotic trajectories to cross.

The torus free barrier is observed in all phase spaces of Fig. 4. In Fig. 4(a), we show the phase space for a parameter corresponding to a no-barrier, no-transport scenario for $n_f = 10^2$. In this case, transport occurs between $n_f = 10^2$ and $n_f = 10^3$. In Fig. 4(b), transport occurs between $n_f = 10^3$ and $n_f = 10^4$, while in the last case, transport only occurs for $n_f > 10^4$. Comparing all the panels from Fig. 4, we observe that the sizes of resonance zones are different. As defined in [27], a resonance zone is a closed region bounded by alternating segments of the stable and unstable manifolds of hyperbolic points. The size of such zones are related with the the flux of trajectories escaping from the resonance zone [28].

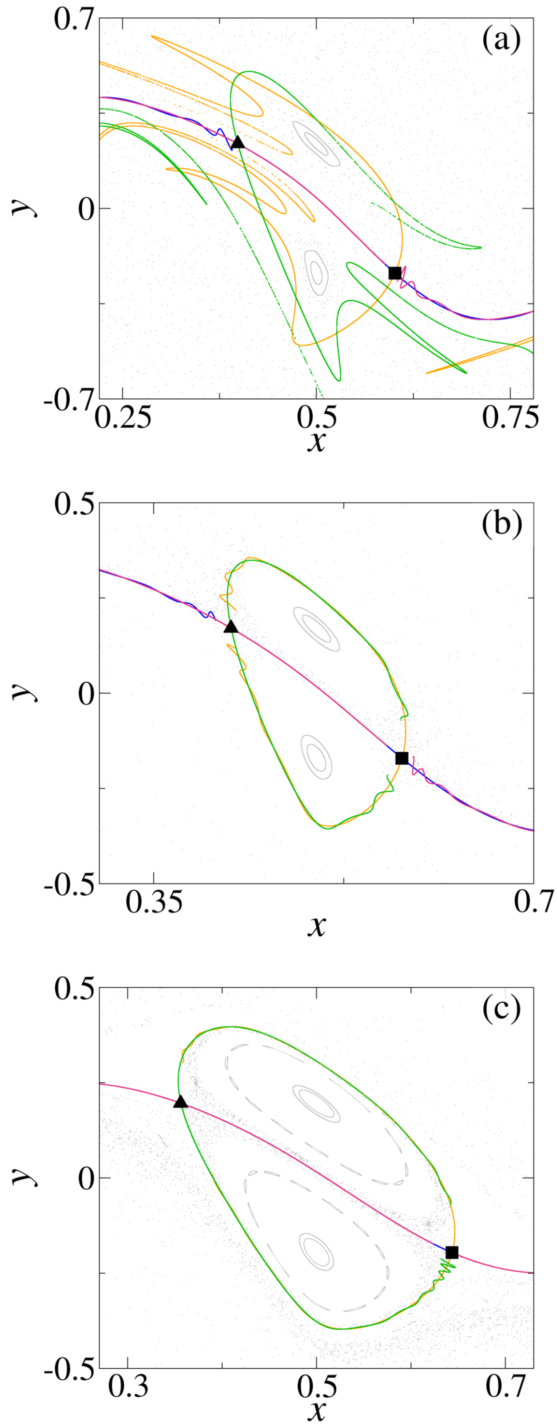

FIG. 4. Manifold structures for even periods. The stable manifold for the hyperbolic point $\mathbf{O}^{\blacktriangle}$ ($\mathbf{O}^{\blacksquare}$) is indicated in blue (green) while the unstable manifolds for the same hyperbolic points are depicted in orange (magenta). The parameters for each panel are (a) $(a, b) = (0.53, 0.8)$, (b) $(a, b) = (0.515, 0.72)$, and (c) $(a, b) = (0.52, 0.5)$.

Following this reasoning, transport is expected to occur more readily in the scenario shown in Fig. 4(a), since the resonance zones are larger. For the parameters in larger iteration time regions, the resonance zones are smaller, indicating a reduced flux through them. As shown in Ref. [7], the flux

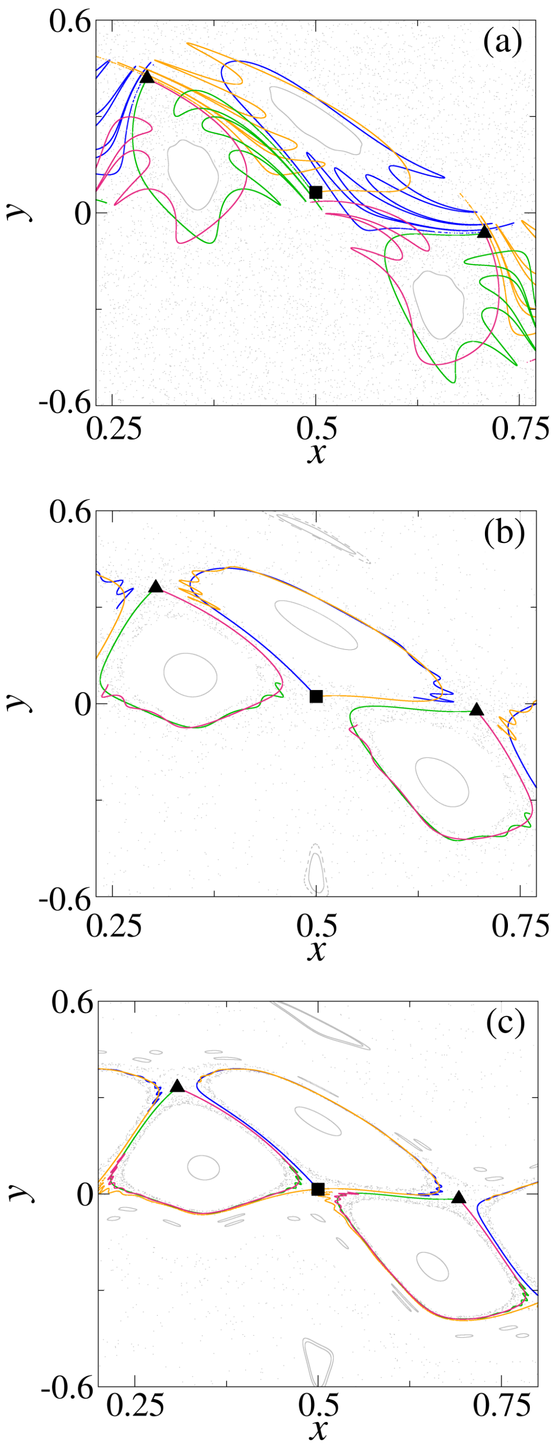

FIG. 5. Turnstile structures in the period-3 scenario. The chosen parameters are (a) $a = 0.71$ and $b = 0.5$, (b) $a = 0.697$ and $b = 0.405$, and (c) $a = 0.6921$ and $b = 0, 3707$. We follow the same color scheme for the stable and unstable manifolds as in Fig. 4.

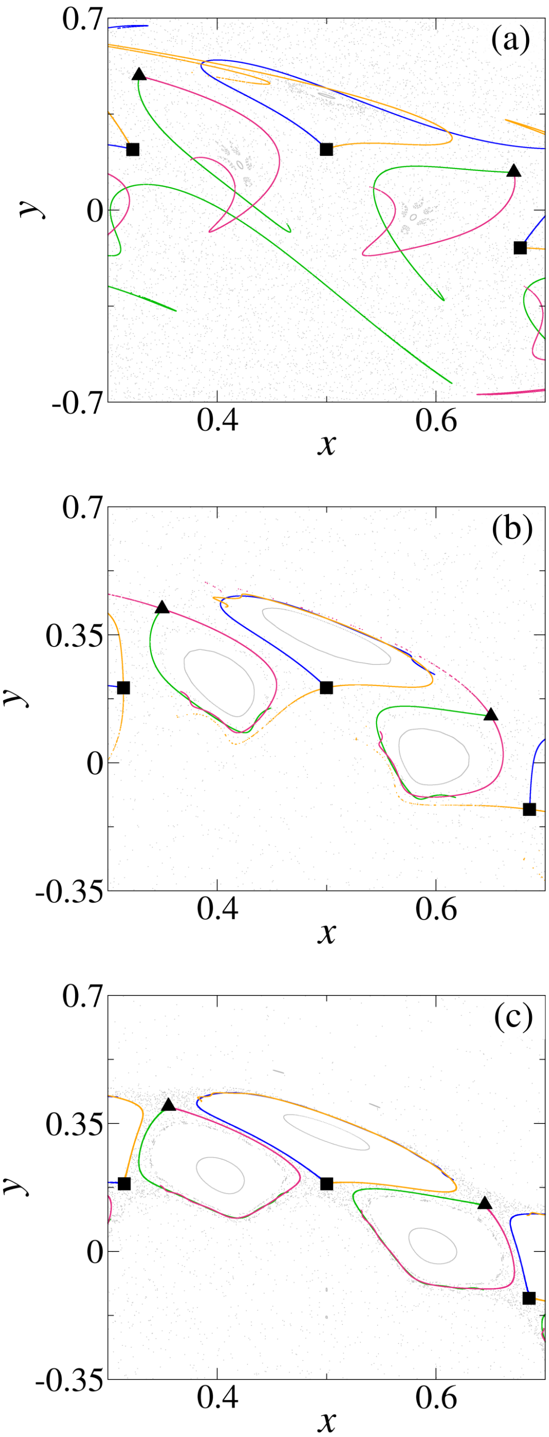

FIG. 6. Manifold structures for the period-5 scenario. For panel (a), we have $(a, b) = (0.865, 0.4)$ while for panels (b),(c) we have $(a, b) = (0.85, 0.362)$ and (0.8437,0.3409), respectively. The same color scheme used for the stable and unstable manifolds in Figs. 4 and 5 is adopted here.

occurs through the resonance zones located in the middle of the structure, i.e., those formed by the blue and magenta manifolds. These zones also decrease in size as for parameters in regions with larger iteration time n_f, as shown sequentially in Figs. 4(a)–4(c). With smaller resonance zones, the partial barrier becomes more efficient.

For an odd period, the manifold structure is different and is known as a *turnstile* [3,6,8,29]. Turnstiles are lobes of the structure formed by the stable and unstable manifolds of a hyperbolic point, acting as a revolving door that enables transport across the region. For a detailed and comprehensive review of this concept, see Ref. [8].

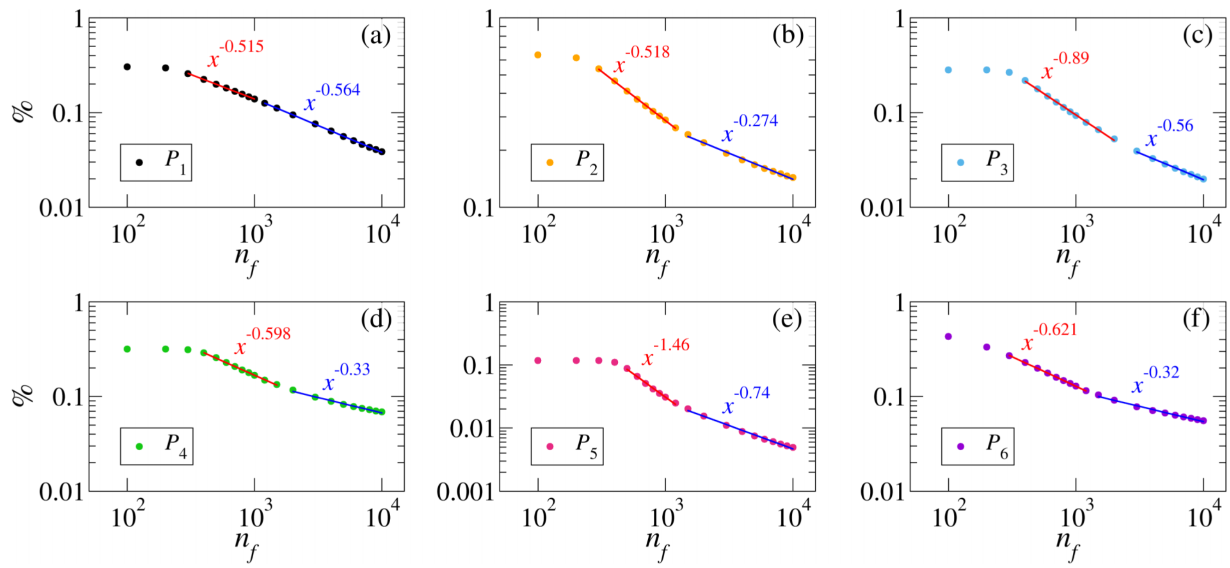

FIG. 7. Relative size of the no-barrier, no-transport regions for the parameter space regions in Fig. 3, as a function of the final iteration time n_f. The data are presented on a log-log scale, where two distinct regimes can be identified. The solid lines indicate power-law fits, with the corresponding exponents shown in each panel. We observe two distinct exponents in each panel, indicating different scaling behaviors and functional dependences as n_f increases. The exponent values for each period highlight the influence of the island period on the decay rate. The period for each panel is indicated in the legend.

We chose the period-3 case as the first representative of an odd period, corresponding to the scenario shown in Fig. 3(a_3). The phase space, the period-3 hyperbolic points, and the corresponding manifolds for the three pair of parameters marked in Fig. 3(a_3) are presented in Fig. 5. For better visualization, we show a magnified view around the islands centered at $x = 0.5$.

In all panels of Fig. 5, we observe turnstile structures. The manifolds from the lower (upper) hyperbolic points, represented by the black square and black triangle, respectively, encompass the island from the upper (lower) chain. Similarly to what is observed in Fig. 4, the sizes of the resonance zones are different in each panel; they are larger in Fig. 5(a), which corresponds to the scenario in the shorter iteration time region. The size of the resonance zones decreases for parameters chosen in longer iteration time regions, as seen when comparing Figs. 5(b) and 5(c) with Fig. 5(a). Consequently, the flux is reduced in the phase space of panels (b), (c) of Fig. 5, requiring a larger n_f for a transport scenario. Furthermore, we observe the intercrossing scenario in Fig. 5(a) that it is not observed in panels (b), (c). The intercrossing scenario is formed by heteroclinic points resulting from the intersections between manifolds from different hyperbolic points. As stated in previous studies [4–6], this scenario enhances transport, resulting in higher transmissivity through phase space.

Finally, we present the last scenario observed for odd-period islands. We choose the period-5 case as an example, since the period-1 case is similar. The manifold structures for the pairs of parameters chosen in Fig. 3(a_5) are presented in Fig. 6.

A comparison of the manifold structures in Fig. 6 leads to a conclusion similar to that obtained from Fig. 5. When a larger final iteration time n_f is required for transport to occur in phase space, the resonance zones are smaller. In Fig. 6(a), the intercrossing scenario is not observed, yet transport occurs for $n_f > 10^2$. This suggests that the size of the lobes affects transport more strongly than heteroclinic intersections.

V. ROBUSTNESS OF PARTIAL TRANSPORT BARRIERS IN TIME

As a final analysis, we investigate how the no-barrier, no-transport regions shrink with increasing final iteration time. From the parameter spaces in Fig. 3(a), we observe that the orange and magenta regions are larger when the island period is even, i.e., in Fig. 3(a_i), with $i = 2$, 4, and 6. One possible explanation is that the torus free barrier was found to be a strong partial barrier [7], so a larger iteration time is required for transport to occur. Motivated by this observation, we expect the reduction of these regions to exhibit different behaviors depending on whether the island period is even or odd.

To investigate the reduction of the no-barrier, no-transport regions, we compute their sizes, i.e., the number of parameter pairs belonging to these regions relative to the total parameter space, for different final iteration times n_f. In this way, we analyze how the regions in Fig. 3 evolve from the black region to the pink region. The results are presented in Fig. 7.

From the results presented in Fig. 7, we observe distinct decreases in the relative size of the no-barrier, no-transport regions as the final iteration time n_f increases. For all periods, we identify two distinct regimes in the log-log representation. Except for period 1, the decay follows a power law with a larger exponent (red fits) for shorter iteration times, while for larger n_f the decay is described by a power law with a smaller exponent, indicating a slower decay. For period 1, both regimes exhibit similar power-law behavior.

When each regime is considered separately, the exponents for odd periods are larger than those for even periods. This result is related to the robustness of partial barriers. Comparing all periods, the results suggest that partial barriers formed by turnstiles are less robust, as the relative size of the no-barrier, no-transport regions decreases more rapidly for larger iteration time. In contrast, for even periods, this decrease is slower, indicating that the barriers remain more effective even for longer iteration times. This is consistent with the findings in Ref. [7], where it was shown that longer iteration times are required for chaotic trajectories to cross the torus free barrier structure.

With these findings, we can conclude that the variation in the exponents across the panels of Fig. 7 highlights the influence of the island period on the robustness of the partial barriers. Since the period determines the manifold structure, it also sets the flux of chaotic trajectories through phase space and, consequently, controls the transport properties of the system.

VI. CONCLUSIONS

Transport through phase space in Hamiltonian systems can be reduced or even suppressed by the presence of partial barriers. For different parameter values and final iteration times, the transmissivity, a quantity related to the fraction of chaotic trajectories that cross phase space, varies and may even vanish for certain parameter sets. This can be verified through the evaluation of the transmissivity and the observation of the evolution of chaotic trajectories in phase space.

By computing the parameter space for the existence of the shearless curve using the method proposed in Ref. [17], based on indicator points, we identify the parameter pairs for which a complete transport barrier exists and transport is fully suppressed. Furthermore, we obtain the parameter pairs for which the shearless barrier is absent and the transport of chaotic trajectories is a possible scenario. By evaluating the transmissivity for parameter pairs without a complete barrier, we obtain the parameter space characterizing the intensity of transport through phase space. This parameter space contains points corresponding to the no-barrier, no-transport scenario, where transport does not occur even in the absence of a barrier. This region decreases as the final iteration time increases, but does not disappear completely.

Through an analysis of the period of the twin islands in phase space, we identify a correlation between the size of the no-barrier, no-transport regions and the parity of the islands. For odd periods, these regions are smaller compared to those observed for even periods. From a manifold perspective, we explain this difference in terms of the underlying manifold structures of these scenarios. For odd periods, turnstile structures enable transport through the flux across their lobes. In contrast, for even periods, torus free barriers act as more effective partial barriers, preventing transport through phase space. In this case, even long iteration times are not sufficient for transport to occur. As a result, the no-barrier, no-transport regions are larger in parameter space for even periods.

To confirm the relationship between periodicity and the no-barrier, no-transport regions in parameter space, and to analyze the robustness of partial barriers formed by turnstiles (odd-period scenarios) and torus free barriers (even-period scenarios), we compute the decay of the relative size of these regions for different values of the final iteration time. Our results show that the power-law decay of the no-barrier, no-transport regions has different exponents for odd and even periods, with larger values for odd periods than for even ones, indicating that partial barriers are less efficient for odd periods than for even ones at the same final iteration time.

From the periodicity and manifold analyses, together with the analysis of the shrinkage of the no-barrier, no-transport regions in parameter space, we can explain the “false positives” in the transmissivity parameter space, i.e., points that indicate no transport but do not correspond to a complete barrier. With this in mind, it is important to compute the parameter space for the existence of the shearless curve (the total barrier) using the method based on indicator points, instead of using transmissivity.

ACKNOWLEDGMENTS

This research received the support of São Paulo Research Foundation (FAPESP, Brazil), under Grants No. 2023/08698-9 and No. 2024/05700-5; the National Council for Scientific and Technological Development (CNPq, Brazil), under Grants No. 302665/2017-0 and No. 309670/2023-3; and the Paraná Research Foundation (Fundação Araucária). E.D.L. acknowledges support from CNPq (Grants No. 301318/2019-0 and No. 304398/2023-3) and the Fundação de Amparo à Pesquisa do Estado de São Paulo (FAPESP) (Grants No. 2019/14038-6 and No. 2021/09519-5). The computational simulations in this research were supported by resources supplied by the Center for Scientific Computing (NCC/GridUNESP) of the São Paulo State University (UNESP) and by the Oscillations Control Group [30] of the University of São Paulo. We would also like to thank the 105 Group Science [31] for fruitful discussions.

DATA AVAILABILITY

The data that support the findings of this article are openly available [32].

[1] A. J. Lichtenberg and M. A. Lieberman, *Regular and Chaotic Dynamics* (Springer Science & Business Media, Berlin, 2013), Vol 38.

[2] R. S. Mackay, J. Meiss, and I. Percival, Transport in Hamiltonian systems, Physica D **13**, 55 (1984).

[3] R. S. MacKay, J. D. Meiss, and I. C. Percival, Stochasticity and transport in Hamiltonian systems, Phys. Rev. Lett. **52**, 697 (1984).

[4] J. D. Szezech, I. L. Caldas, S. R. Lopes, R. L. Viana, and P. J. Morrison, Transport properties in nontwist area-preserving maps, Chaos **19**, 043108 (2009).

[5] J. D. Szezech, Jr., I. L. Caldas, S. R. Lopes, P. J. Morrison, and R. L. Viana, Effective transport barriers in nontwist systems, Phys. Rev. E **86**, 036206 (2012).

[6] M. Mugnaine, A. C. Mathias, M. S. Santos, A. M. Batista, J. D. Szezech, Jr., and R. L. Viana, Dynamical characterization of transport barriers in nontwist Hamiltonian systems, Phys. Rev. E **97**, 012214 (2018).

[7] M. Mugnaine, I. L. Caldas, J. D. Szezech, Jr., R. L. Viana, and P. J. Morrison, Shearless effective barriers to chaotic transport induced by even twin islands in nontwist systems, Phys. Rev. E **110**, 044201 (2024).

[8] J. Meiss, Thirty years of turnstiles and transport, Chaos **25**, 097602 (2015).
[9] B. V. Chirikov, A universal instability of many-dimensional oscillator systems, Phys. Rep. **52**, 263 (1979).
[10] J. M. Greene, A method for determining a stochastic transition, J. Math. Phys. **20**, 1183 (1979).
[11] R. MacKay, A renormalization approach to invariant circles in area-preserving maps, Physica D **7**, 283 (1983).
[12] S. Aubry, The twist map, the extended Frenkel-Kontorova model and the devil's staircase, Physica D **7**, 240 (1983).
[13] J. D. Meiss, Symplectic maps, variational principles, and transport, Rev. Mod. Phys. **64**, 795 (1992).
[14] D. del-Castillo-Negrete and P. Morrison, Chaotic transport by Rossby waves in shear flow, Phys. Fluids **5**, 948 (1993).
[15] D. del-Castillo-Negrete, J. M. Greene, and P. J. Morrison, Area preserving nontwist maps: Periodic orbits and transition to chaos, Physica D **91**, 1 (1996).
[16] I. L. Caldas, Jr., R. Viana, J. Szezech, J. Portela, J. Fonseca, M. Roberto, C. Martins, and E. da Silva, Nontwist symplectic maps in tokamaks, Commun. Nonlinear Sci. Numer. Simul. **17**, 2021 (2012).
[17] A. Wurm, A. Apte, and P. J. Morrison, On reconnection phenomena in the standard nontwist map, Braz. J. Phys. **34**, 1700 (2004).
[18] S. Shinohara and Y. Aizawa, Indicators of reconnection processes and transition to global chaos in nontwist maps, Prog. Theor. Phys. **100**, 219 (1998).
[19] A. Wurm, A. Apte, K. Fuchss, and P. J. Morrison, Meanders and reconnection–collision sequences in the standard nontwist map, Chaos **15**, 023108 (2005).
[20] R. L. Viana, I. L. Caldas, J. D. Szezech, Jr., A. M. Batista, C. Abud, A. B. Schelin, M. Mugnaine, M. S. Santos, B. B. Leal, B. Bartoloni, *et al.*, Transport barriers in symplectic maps, Braz. J. Phys. **51**, 899 (2021).
[21] A. C. Mathias, M. Mugnaine, M. S. Santos, J. D. Szezech Jr, I. L. Caldas, and R. L. Viana, Fractal structures in the parameter space of nontwist area-preserving maps, Phys. Rev. E **100**, 052207 (2019).
[22] D. del-Castillo-Negrete, J. Greene, and P. Morrison, Renormalization and transition to chaos in area preserving nontwist maps, Physica D **100**, 311 (1997).
[23] P. J. Morrison, Magnetic field lines, Hamiltonian dynamics, and nontwist systems, Phys. Plasmas **7**, 2279 (2000).
[24] E. Petrisor, Nontwist area preserving maps with reversing symmetry group, Int. J. Bifurcation Chaos **11**, 497 (2001).
[25] D. Hobson, An efficient method for computing invariant manifolds of planar maps, J. Comput. Phys. **104**, 14 (1993).
[26] G. Corso and F. B. Rizzato, Manifold reconnection in chaotic regimes, Phys. Rev. E **58**, 8013 (1998).
[27] R. W. Easton, Transport through chaos, Nonlinearity **4**, 583 (1991).
[28] H. E. Lomelí and J. D. Meiss, Resonance zones and lobe volumes for exact volume-preserving maps, Nonlinearity **22**, 1761 (2009).
[29] V. Rom-Kedar, A. Leonard, and S. Wiggins, An analytical study of transport, mixing and chaos in an unsteady vortical flow, J. Fluid Mech. **214**, 347 (1990).
[30] https://web.if.usp.br/controle/.
[31] https://www.105groupscience.com.
[32] http://henon.if.usp.br/OscilControlData/FalsePositives/.